Author(s): Latifi, Kourosh & Wijaya, Harri & Zhou, Quan

Title: Motion of Heavy Particles on a Submerged Chladni Plate

Year: 2019

Version: Final published version

Please cite the original version:

Latifi, Kourosh & Wijaya, Harri & Zhou, Quan. 2019. Motion of Heavy Particles on a Submerged Chladni Plate. Physical Review Letters. Volume 122, Issue 18. 5. DOI: 10.1103/PhysRevLett.122.184301.

Editors' Suggestion | Featured in Physics

Motion of Heavy Particles on a Submerged Chladni Plate

Kourosh Latifi, Harri Wijaya, and Quan Zhou*
Department of Electrical Engineering and Automation, Aalto University, Espoo 02150, Finland

(Received 28 January 2019; published 10 May 2019)

Heavy particles are traditionally believed to gather at the nodes of a resonating plate, forming standard Chladni patterns. Here, for the first time, we experimentally show that heavy particles, i.e., sub-mm particles, can move towards the antinodes of a resonating plate. By submerging the resonating plate inside a fluidic medium, the acoustic radiation force and the lateral effective weight become dominant at the sub-mm scale. Those forces, averaged over a vibration cycle, move the particles towards the antinodes and generate sophisticated patterns. We create a statistical model that relates the complex motion of particles to their locations and plate vibration frequencies in a wide spectrum of both resonant and nonresonant frequencies. Additionally, we employ our model to control the motion of single particles and a swarm of particles on the submerged plate. Our device can move particles with sufficient power at an exceptionally wide frequency range, potentially opening a path to new particle manipulation techniques at sub-mm scale in fluidic media.

DOI: 10.1103/PhysRevLett.122.184301

Understanding how particles move on a vibrating plate has been a critical milestone in acoustics. In 1787, Ernst Chladni, known as the father of acoustics, sprinkled sand particles on a thin centrally-mounted plate and drew a violin bow over the edge of the plate. He showed that the sand particles move and settle on the nodes of vibration, forming Chladni patterns [1]. He also reported that very fine particles, shavings from his violin bow, move to the antinodes of vibration and form inverse Chladni patterns. Faraday showed that the latter behavior was caused by air currents in the vicinity of the plate, now known as acoustic streaming [2]. Since then, the dominant view has been that heavy particles gather at the nodes, and light particles collect at the antinodes of a resonating plate [3,4], except a simulation study [5]. Additionally, all the reported experiments support this dominant view.

In this Letter, we show for the first time that heavy particles can move towards the antinodes of vibration. We place heavy particles, e.g., sub-mm glass beads, on a submerged vibrating plate. In such a system, fluid drag force keeps the particles mostly attached to the surface of the plate with relative low vibration amplitude. Meanwhile, the acoustic radiation force [6] and the lateral component of the effective weight [5] drive the particle towards the antinodes. To understand the motion of the particles, we create a statistical model of such motion in relation to the spatial location of the particle at given frequencies. The statistical model covers a wide spectrum of frequencies, including both resonant and nonresonant.

Additionally, we employ our statistical model to dynamically control the motion of single particles and a swarm of particles on the submerged Chladni plate. This potentially paves the way to new particle manipulation techniques at sub-mm scale inside a fluidic medium. Compared to other acoustofluidic techniques that generally work with suspended particles [7], our method facilitates direct actuation of the particles on the surface. Furthermore, unlike other acoustofluidic techniques that usually work at the narrow bandwidths defined by the resonant frequencies of the structure [7–12], our device generates sufficient power to move particles at a wide spectrum of frequencies, allowing versatile and diverse motion control, which potentially impacts procedures in biomedical and pharmaceutical research, tissue engineering, and microsystem assembly.

The apparatus consists of a centrally-actuated vibrating plate submerged in a water tank, as shown in Fig. 1(a). The vibrating plate has dimensions of $50\ \text{mm} \times 50\ \text{mm} \times 500\ \mu\text{m}$, diced from a silicon wafer and glued on a piezoelectric actuator (Piezomechanik, PSt $150/2 \times 3/20$) using a cyanoacrylate adhesive. The piezoelectric actuator is mounted on a dual-axis goniometer (Thorlabs, GN2/M). The electrical connections are insulated using a coating spray (PRF 202). The whole structure is placed inside a tank filled with deionized water. We use glass beads (Retsch, nominal diameter 750 μm) as manipulation specimens. The particles and plate are imaged from above by a video camera (ImperX, IGV-B1621C-KC000 with Infinity/InfiniMite Alpha lens). The plate is excited with sinusoidal signals at a frequency between 523 Hz to 29834 Hz. The excitation signal is generated in a personal computer, passed through a digital-to-analog converter (National Instruments, USB-6363), amplified by a linear amplifier (Piezo Systems, EPA-104-230), and sent to the piezoelectric actuator.

In our system, the motion of the particles involves surface contact, as shown in Video SM1. Therefore, two distinct mechanisms drive the particles towards the

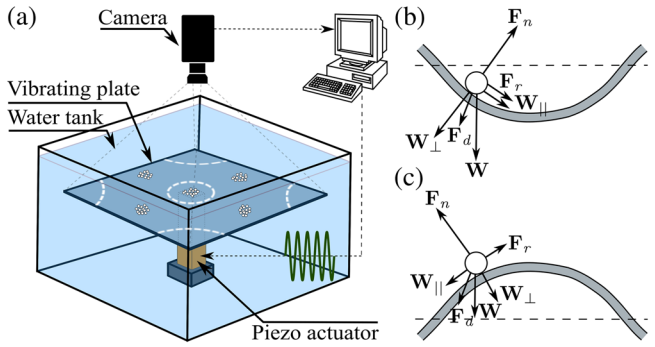

FIG. 1. (a) Schematic of the experimental device: a silicon plate is mounted on a piezoelectric actuator and submerged in a water tank. A computer generates a signal that excites the submerged plate and moves the particles on the plate towards the antinodes. The white dashed lines represent the nodal lines. (b) and (c) Acting forces on a particle on the submerged Chladni plate at two moments during a vibration cycle where in (b) the lateral effective weight ($\langle \mathbf{W}_{||} \rangle$) is larger than in (c). The acoustic radiation force $\mathbf{F}_r$ points towards the antinodes, and the drag force $\mathbf{F}_d$ acts in a direction that is opposite to the motion of the particle during the whole vibration cycle.

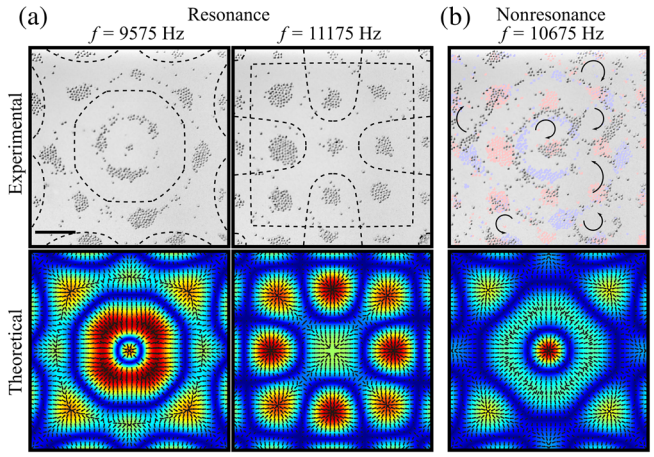

FIG. 2. (a) Experimental and theoretical resonant patterns: in the experimental figures (first row), the black dashed lines are overlaid for better visualization of the nodal lines. In the theoretical figures (second row), the time-averaged horizontal effective weight $\langle \mathbf{W}_{||} \rangle$ (arrows) is overlaid on the theoretical vibration amplitude ξ, where the force points towards the antinodes. (b) Experimental and theoretical nonresonant patterns: in the experimental figure, arrows show the vortexlike motion path. It follows that the adjacent resonant patterns, which are underlaid in the experimental figure, affect the path of the vortexlike motion. Scale bar, 10 mm.

antinodes, as shown in Figs. 1(b) and 1(c). The first mechanism involves the acoustophoretic motion of particles towards the antinodal regions of vibration [6]. The second mechanism is triggered by vibrational acceleration of the plate where the particle mostly remains in contact with the plate [5]. The combination of these forces leads to the motion of the particles that is mostly sliding or rolling on the plate surface with occasional bouncing, as shown in the video SM1 in Supplemental Material [13]. Other mechanisms such as acoustic streaming is negligible considering the size and density of the particle.

We firstly investigated the motion patterns at resonant frequencies of the plate, both experimentally and theoretically. The experimental results are in good correspondence with the theory [Fig. 2(a)]. At resonant frequencies, particles move towards the antinodal regions of the plate, and form stable and predictable inverse Chladni patterns. Figure 2(a), first row, shows two resonant modes occurring in our experiments at 9575 and 11 175 Hz, where the particles gather on antinodal regions of the plate. We simulated the antinodal regions by solving inhomogeneous Helmholtz equation for a centrally-actuated time-harmonic damped plate [14]. We obtained the complex response function of the plate $\psi(x, y)$, and by normalizing the response function magnitude $|\psi|$ with respect to the actual vibration amplitude of the center point, we calculated the theoretical vibration amplitude of the plate $\xi(x, y)$ (see Supplemental Material for detailed explanation [13]). Figure 2(a), second row, shows the theoretical vibration amplitude (ξ) in color. The local maxima of ξ, underlaid by the hot color in the plots, correspond to the antinodal regions of the plate.

The motion of the particles on the plate is driven by two mechanisms as shown in Figs. 1(b) and 1(c). The first mechanism involves the acoustophoretic motion of particles, including acoustic radiation and drag-induced acoustic streaming forces. However, since we manipulate heavy and large particles, acoustic streaming does not contribute significantly in our system [4]. We calculated acoustic radiation force $\mathbf{F}_r$ by employing the method explained in Ref. [6], and showed that it points towards the antinodes. We established a standing wave field on the vibrating interface with ξ, which generates an acoustic pressure field in the fluid. Such pressure field applies acoustic radiation force to the particles that can be calculated from the Gorkov equation [15] (see Supplemental Material [13] for detailed explanation of our simulations). It is noteworthy that, as we excite the system in subsonic regime, the acoustic pressure decays with the increase in distance from the plate. This implies that the pressure change is highly local and near the surface of the plate, and the boundary conditions of other interfaces, such as the fluid-air-interface, does not influence the forces noticeably.

In the second mechanism, the vibrational motion of the plate affects the particle effective weight $\mathbf{W}$,

$$\mathbf{W}(x, y, t) = -m[g + \ddot{z}(x, y, t)] - \mathbf{F}_{\mathrm{dz}}, \tag{1}$$

where (x, y) denotes the spatial location of the particle on the plate, m the mass of the particle, g the gravitational acceleration, $\mathbf{F}_{\mathrm{dz}}$ the vertical drag force, and z the vertical

deflection of the plate at (x, y). As long as the particle does not detach from the plate, the parallel component of $\mathbf{W}$ to the plate ($\mathbf{W}_{||}$), averaged over a complete vibration cycle, points towards the antinodes [5]. We calculate the time averaged of such force over a vibration cycle as below,

$$\langle \mathbf{W}_{||} \rangle (x, y, t) = \frac{\omega}{2\pi} \int_0^{\omega/2\pi} \mathbf{W}(x, y, t) \frac{dz(x, y, t)}{dx} dt, \quad (2)$$

where ω denotes the angular velocity of vibration and $\mathbf{W}_{||x}$ the parallel component of the effective weight in x direction (see Supplemental Material [13] for a detailed explanation). The total parallel component of the effective weight, $\mathbf{W}_{||}$, is then calculated by adding $\mathbf{W}_{||x}$ and $\mathbf{W}_{||y}$. Figure 2(a), second row, shows $\langle \mathbf{W}_{||} \rangle$ (arrows) overlaid on ξ. The results show that $\langle \mathbf{W}_{||} \rangle$ is oriented towards the antinodal regions of vibration as well.

Although resonant patterns can be modeled theoretically, the aforementioned methods are not able to explain the nonresonant patterns, as is evident from Fig. 2(b). Notably, in specific nonresonant frequencies, we observed a farandolelike particle motion as also was reported by Vuillermet *et al.* [3]. In this motion, particles move in a global or local vortexlike trajectory, in the manner of a farandole dance. Unlike the experimental evidence, theoretical methods do not explain any vortical motion of particles on the plate. We attribute the farandolelike motion to the shape of the adjacent resonant modes, the frequencies of which are close enough to the exciting nonresonant frequency. Figure 2(b) shows the farandolelike motion occurring at 10 675 Hz, overlaid on the inverse Chladni patterns formed at two adjacent resonant frequencies, namely 9575 and 11 175 Hz. See Video SM2 in the Supplemental Material [13] for better visualization of farandolelike motion, and the effect of adjacent resonant modes.

To quantitatively describe the particle motion on the plate, especially in nonresonant frequencies, we applied particle tracking velocimetry [16] to build models that can estimate the motion of particles at a given location and frequency (see Fig. 3). Remarkably, our setup generates sufficient power to move particles at almost any frequency in the range of 500 to 30 000 Hz. To cover the frequency range, we chose chromatic musical scale resulting in 71 distinct frequencies, or notes, including both resonant and nonresonant. We have constructed models for all of the 71 notes. To build the models, we evenly placed a cluster of glass beads (ϕ750 μm) on the plate and played a note. We tracked the positions of the particles before and after playing the note. We performed such experiment 25 times for each note, resulting in average 3848 data points per note. Then, we created a database of the notes, positions, and resulting displacements. For each note, we fit a model $\mathbf{d}_n(x, y)$ to the data,

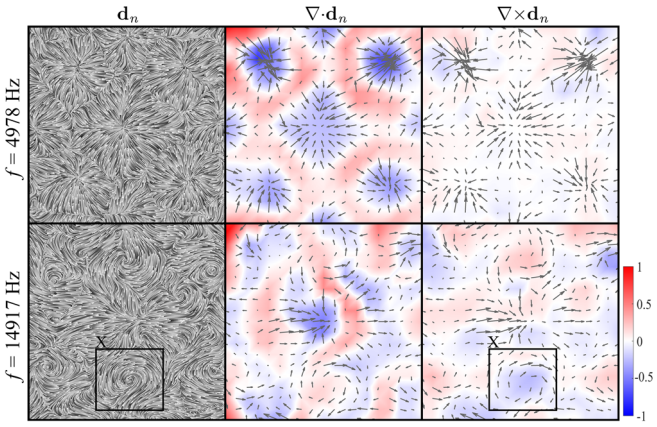

FIG. 3. Modeled displacement fields: first column shows the evenly spaced streamlines of the displacement field $\mathbf{d}_n(x, y)$ at 4978 and 14 917 Hz. Second column shows the divergence of the displacement field underlaid below the modeled displacement vector field, whereby the red and blue regions represent the nodal and antinodal regions of vibration, respectively. Third column shows the signed magnitude of curl, overlaid on the corresponding displacement field. Inset X indicates a spot with a clockwise vortical motion.

$$(\Delta x, \Delta y) = \mathbf{d}_n(x, y) + \mathbf{r}_n(x, y), \quad (3)$$

where Δx and Δy denote the measured displacement of the particle in x and y directions, and $\mathbf{d}_n$ and $\mathbf{r}_n$ the modeled displacement and uncertainty for the note n, respectively. $\mathbf{d}_n$ estimates the expected displacement of a particle at location (x, y), given that the note n is played for a duration of 500 ms. The uncertainty $\mathbf{r}_n$ can be estimated by calculating the difference between the measured and expected displacement (see Supplemental Material [13] for the detailed explanation of the modeling method). Consequently, $\mathbf{r}_n$ determines how random the motion would be at location (x, y) after playing note n. We applied line integral convolution [17] to visualize the displacement fields by evenly spaced streamlines (Fig. 3, first column). The complete set of the 71 displacement fields are shown in Supplemental Fig. 5 in Supplemental Material [13].

The nodal, antinodal, and vortical regions of the motion can be identified mathematically from the displacement field, in terms of divergence and curl. We detect the nodal and antinodal regions of the plate by calculating the divergence of the modeled vector fields,

$$\nabla \cdot \mathbf{d}_n = \frac{\partial u}{\partial x} + \frac{\partial v}{\partial y}, \quad (4)$$

where u and v are the displacement components in x and y directions. Local minima of the divergence represents the antinodal regions, and local maxima of the divergence represents the vibrational nodal lines. Figure 3, second column, shows the modeled displacement field $\mathbf{d}_n$ underlaid by the divergence for two frequencies, 4978 and

14 917 Hz, where blue and red colors represent the nodal and antinodal regions of vibration, respectively. See Supplemental Fig. 5 in the Supplemental Material [13] for the divergence plots of all notes. We identify the spots where particles translate in a vortexlike trajectory by calculating the curl of the displacement field $\mathbf{d}_n$,

$$\nabla \times \mathbf{d}_n = \left(\frac{\partial v}{\partial x} - \frac{\partial u}{\partial y}\right)\hat{\mathbf{k}}, \tag{5}$$

where curl of $\mathbf{d}_n$ represents the magnitude and direction of a vortex. The higher the magnitude of the curl, the higher the tendency of particles to rotate around that spot. The direction of the curl specifies the direction of the vortical motion, whereby a positive value represents a clockwise vortical motion, and a negative value represents a counterclockwise vortical motion of the particles. As shown in Fig. 3, third column, curl captures the spots in which particles tend to move in a vortex-like trajectory. See Supplemental Fig. 5 in the Supplemental Material [13] for the curl plots of all notes.

We noticed that the magnitude of curl compared to divergence generally increases with frequency. To understand the contribution of divergence and curl at different frequencies, we define the scalar η as the ratio of curl to divergence for each note as follows,

$$\eta = \frac{\iint_T |\nabla \times \mathbf{d}_n| dxdy}{\iint_T |\nabla \cdot \mathbf{d}_n| dxdy}, \tag{6}$$

where T denotes the plate surface. We observed that η generally increases for our manipulation frequencies (see Supplemental Fig. 6 in the Supplemental Material [13]). In higher frequencies, the acoustic wavelength is shorter, and consequently, the number of waves increases over the plate. Thus, we observe more frequent changes in the directions of the vector field at higher frequencies, resulting in higher values of η.

The modeled displacement fields provide detailed information about the particle motion at different excitation frequencies. We exploit such excitation fields to control the motion of particles on the plate with a high degree of freedom. This allows manipulation of particles to achieve complicated tasks such as moving a particle in a maze, and following specific trajectories. We have successfully manipulated a $\phi 750$ μm glass bead on a maze-shaped trajectory [Fig. 4(a) and Video SM3 in the Supplemental Material [13]]. To control the motion of the particle, we split the trajectory into a set of waypoints. We use a sequence of notes to direct the object to its current waypoint. In each step of the sequence, a camera measures the current position of the particle. The measured position is fed to a closed-loop control algorithm [16]. The algorithm searches in the database of the modeled notes, and selects the note that directs the particle towards the waypoint (see Supplemental Material [13] for the detailed explanation of the control algorithm). The selected note is played on the vibrating plate, which induces the desired displacement field to move the particle. The algorithm runs the measure-calculate-play steps until the distance between the particle and its waypoint is less than a predefined threshold. Then the algorithm directs the particle towards the next waypoint along the trajectory.

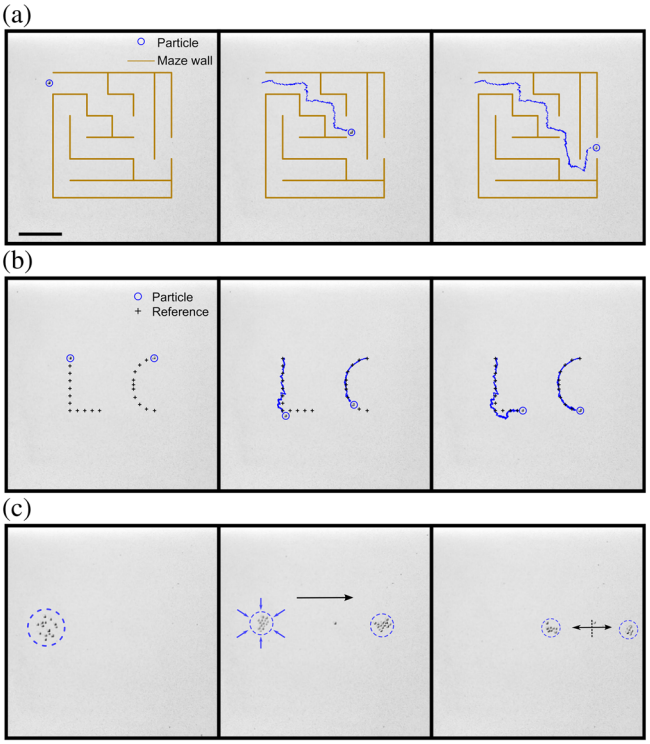

FIG. 4. Manipulation of single particles and a swarm of particles: (a) Manipulation of a 750 μm glass bead on a maze-shaped trajectory (Video SM3). (b) Simultaneous and independent manipulation of two 750 μm glass beads on two predefined trajectories resembling the letters of L and C (Video SM4). (c) Manipulation of a swarm of particles (Video SM5): placing multiple particles on the plate, aggregating them into a bundle, transporting the swarm of particles towards the center and then to the splitting location and splitting them into two clusters of particles. Scale bar, 10 mm.

We have also applied our method to manipulate multiple particles simultaneously and independently. We simultaneously manipulated two particles on two predefined trajectories resembling the letters of L and C [Fig. 4(b) and Video SM4 in the Supplemental Material [13]]. We split each trajectory into a set of waypoints, and move each particle towards its current waypoint, similar to the first manipulation test. When both of the particles reach their current waypoints, the algorithm directs the particles towards the next waypoints.

Besides single particle manipulation, we have also successfully demonstrated the merging, transportation, and separation of a swarm of particles [Fig. 4(c) and Video SM5 in the Supplemental Material [13]]. The experiment started by placing a swarm of particles near the start location on the plate. We selected a proper note,

A_8, from the displacement field database to merge the particles together. We then excited another note, $G_5^{\#}$, to transport the swarm towards the center of the plate. We replayed the note A_8 to aggregate the particles in the center of the plate, and transported the particles towards the splitting point using the note $G_5^{\#}$. Finally, we excited the note $C_7^{\#}$ to split the particles into two distinct groups.

In this Letter, for the first time we have shown an experimental case where heavy particles move towards the antinodes of a resonating plate, by submerging the plate inside water. Furthermore, we have explained the diverse and complex motion of particles on such a submerged Chladni plate by a statistical model, which accurately describes the motion in both resonant and nonresonant frequencies. Based on the statistical model, we have further analyzed the motion patterns in terms of divergence and curl. This gives a better understanding about the behavior of heavy particles in such a system. Furthermore, we have used the acquired model to control the motion of single particles and a swarm of particles on the plate by simply controlling the excitation frequency. In our experiments, we chose frequencies from western musical scale. Other selection of frequencies can result in a comparable degree of freedom, providing that the selected frequencies cover similar broad spectrum and generate diverse displacement vector fields.

Numerous applications in biological and pharmaceutical research [18–20], tissue engineering [21], microsystem assembly [22], and lab on a chip [7,23] rely on particle manipulation techniques inside a fluidic medium. We believe our manipulation technique has a potential impact in such applications. Our technique has several features that distinguish it from other acoustofluidic techniques. Unlike most reported acoustofluidic techniques that are limited to a finite set of resonant frequencies, our device generates sufficient power to move particles at a wide spectrum of frequencies, including both resonant and nonresonant. The method is not limited to the suspended particles, and facilitates manipulation of heavy particles. It is extremely simple, requiring only a single actuator and no specific micro- and nanostructure on the plate. Despite its simplicity, it is highly versatile, allowing simultaneous and independent manipulation of individual particles or particle swarms. Such a combination of simplicity and versatility can potentially simplify many procedures in biomedical and pharmaceutical research, tissue engineering, and microsystem assembly.

This work was supported by the Academy of Finland (Grant No. 296250), Aalto doctoral school of Electrical Engineering, and LPDP Scholarship of Indonesia. The authors acknowledge Micronova Nanofabrication Centre for providing laboratory facilities for microfabrication, Professor Massimo Mastrangeli and Professor Heikki Nieminen for their insightful comments on the draft of this manuscript, and Zoran Cenev for his comments on mechanical improvement of the bonding of the vibrating plate.

*quan.zhou@aalto.fi

[1] E. F. F. Chladni, *Entdeckungen uber die Theorie des Klanges* (Weidmanns erben und Reich, Leipzig, 1787).
[2] M. Faraday, Phil. Trans. R. Soc. London **121**, 299 (1831).
[3] G. Vuillermet, P.-Y. Gires, F. Casset, and C. Poulain, Phys. Rev. Lett. **116**, 184501 (2016).
[4] H. J. van Gerner, K. van der Weele, M. A. van der Hoef, and D. van der Meer, J. Fluid Mech. **689**, 203 (2011).
[5] H. J. van Gerner, M. A. van der Hoef, D. van der Meer, and K. van der Weele, Phys. Rev. E **82**, 012301 (2010).
[6] J. Lei, Microfluid. Nanofluid. **21**, 50 (2017).
[7] B. W. Drinkwater, Lab Chip **16**, 2360 (2016).
[8] T. Laurell, F. Petersson, and A. Nilsson, Chem. Soc. Rev. **36**, 492 (2007).
[9] M. Wiklund, Lab Chip **12**, 2018 (2012).
[10] J. Shi, X. Mao, D. Ahmed, A. Colletti, and T. J. Huang, Lab Chip **8**, 221 (2008).
[11] J. Shi, D. Ahmed, X. Mao, S.-C. S. Lin, A. Lawit, and T. J. Huang, Lab Chip **9**, 2890 (2009).
[12] Z. Wang and J. Zhe, Lab Chip **11**, 1280 (2011).
[13] See Supplemental Material at http://link.aps.org/supplemental/10.1103/PhysRevLett.122.184301 for the details on the following aspects: fabrication of the vibrating plate, calculation of the theoretical vibration amplitude, analysis of the motion mechanisms and COMSOL simulations, explanation of the high-speed recording of the particle-plate interaction, calculation of nominal amplitude and motion displacement fields, and the control algorithm. Video SM1.mp4 shows the high-speed recording of the particle-plate interaction. Video SM2.mp4 shows the formation of patterns at resonant and non-resonant frequencies. Video SM3.mp4 and SM4.mp4 show the manipulation of single particles on pre-defined trajectories. Video SM5.mp4 shows the manipulation of a swarm of glass beads.
[14] P. H. Tuan, C. P. Wen, P. Y. Chiang, and Y. T. Yu, J. Acoust. Soc. Am. **137**, 2113 (2015).
[15] H. Bruus, Lab Chip **12**, 1014 (2012).
[16] Q. Zhou, V. Sariola, K. Latifi, and V. Liimatainen, Nat. Commun. **7**, 12764 (2016).
[17] B. Jobard and W. Lefer, Creating evenly-spaced streamlines of arbitrary density, in *Visualization in Scientific Computing* (Springer, Vienna, 1997).
[18] P. Y. Chiou, A. T. Ohta, and M. C. Wu, Nature (London) **436**, 370 (2005).
[19] X. Ding, S.-C. S. Lin, B. Kiraly, H. Yue, S. Li, I.-K. Chiang, J. Shi, S. J. Benkovic, and T. J. Huang, Proc. Natl. Acad. Sci. U.S.A. **109**, 11105 (2012).
[20] V. Marx, Nat. Methods **12**, 41 (2015).
[21] S. Li, P. Glynne-Jones, O. G. Andriotis, K. Y. Ching, U. S. Jonnalagadda, R. O. C. Oreffo, M. Hill, and R. S. Tare, Lab Chip **14**, 4475 (2014).
[22] J. Goldowsky, M. Mastrangeli, L. Jacot-Descombes, M. R. Gullo, G. Mermoud, J. Brugger, A. Martinoli, B. J. Nelson, and H. F. Knapp, J. Micromech. Microeng. **23**, 125026 (2013).
[23] P. S. Dittrich and A. Manz, Nat. Rev. Drug Discov. **5**, 210 (2006).